HHS Public Access

Author manuscript

ACS Chem Biol. Author manuscript; available in PMC 2022 March 19.

Published in final edited form as:

ACS Chem Biol. 2021 March 19; 16(3): 480–490. doi:10.1021/acschembio.0c00832.

The structural and biochemical basis of apocarotenoid processing by β-carotene-oxygenase-2

Sepalika Bandara[1], **Linda D. Thomas**[1], **Srinivasagan Ramkumar**[1], **Nimesh Khadka**[1], **Philip D. Kiser**[3,4], **Marcin Golczak**[1,2], **Johannes von Lintig**[1,*]

[1]Department of Pharmacology, Case Western Reserve University, 10900 Euclid Avenue, Cleveland, Ohio 44106, United States of America

[2]Cleveland Center for Membrane and Structural Biology, School of Medicine, Case Western Reserve University, 10900 Euclid Avenue, Cleveland, Ohio 44106, United States of America

[3]Department of Physiology and Biophysics, University of California, Irvine, California 92697

[4]Research Service, Veterans Affairs Long Beach Healthcare System, Long Beach, California 90822.

Abstract

In mammals, carotenoids are converted by two carotenoid cleavage oxygenases into apocarotenoids, including vitamin A. Although knowledge about β-carotene oxygenase-1 (BCO1) and vitamin A metabolism has tremendously increased, the function of β-carotene oxygenase-2 (BCO2) remains less well defined. We here studied the role of BCO2 in the metabolism of long chain β-apocarotenoids, which recently emerged as putative regulatory molecules in mammalian biology. We showed that recombinant murine BCO2 converted the alcohol, aldehyde, and carboxylic acid of a β-apocarotenoid substrate by oxidative cleavage at position C9,C10 into a β-ionone and a diapocarotenoid product. Chain length variation (C20 to C40) and ionone ring site modifications of the apocarotenoid substrate did not impede catalytic activity or altered the regioselectivity of double bond cleavage by BCO2. Isotope labelling experiments revealed that the double bond cleavage of an apocarotenoid followed a dioxygenase reaction mechanism. Structural modeling and site directed mutagenesis identified amino acid residues in the substrate tunnel of BCO2 that are critical for apocarotenoid binding and catalytic processing. Mice deficient for BCO2 accumulated apocarotenoids in their livers, indicating that the enzyme engages in apocarotenoid metabolism. Together, our study provides novel structural and functional insights into BCO2 catalysis and establishes the enzyme as key component of apocarotenoid homeostasis in mice.

*Corresponding author Department of Pharmacology, School of Medicine, Case Western Reserve University, 10900 Euclid Avenue, Cleveland, Ohio 44106, United States of America, Tel: +1 2163683528; Fax: +1 2163681300. johannes.vonlintig@case.edu.

Conflict of interest

The authors declare that they have no conflicts of interest with the contents of this article.

Supporting information

The Supporting Information is available free of charge at http://pubs.acs.org

- mBCO2 catalytic activity with canthaxanthin and various apocarotenoic acids; structural and sequence alignments of mammalian BCO2 proteins, Western blot analysis for the expression levels of mutant BCO2 variants, and control experiments for apocarotenoid composition in mouse tissues.

Graphical abstract

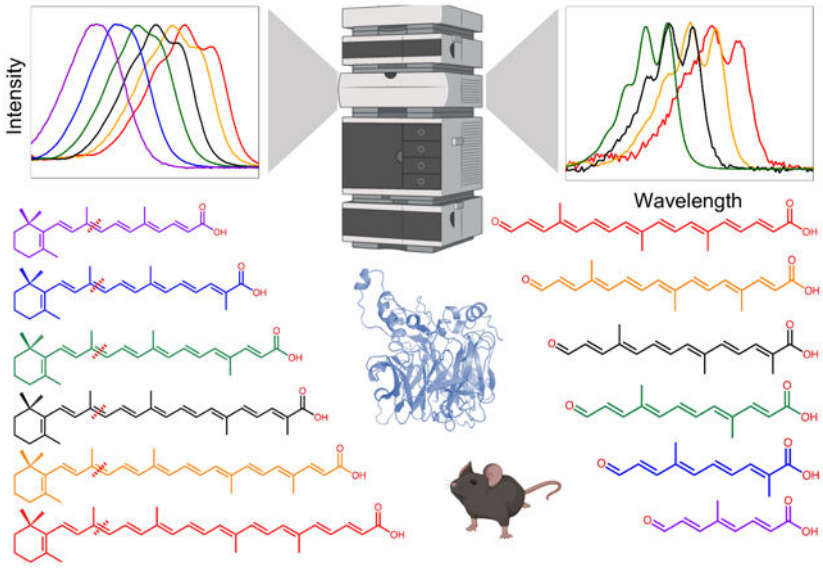

Keywords

metabolism; dioxygenase; carotenoids; apocarotenoids; β-carotene-oxygenase 2 (BCO2)

Introduction

The plant metabolite β-carotene is a significant source of vitamin A (all-*trans*-retinol) in the diet and the precursor for at least two biologically active metabolites: 11-*cis*-retinal is the chromophore of visual pigments in photoreceptors of the eyes [1], and all-*trans*-retinoic acid (RA) is a hormone-like compound in most tissues [2]. 11-*cis*-Retinal binds to sensory G-protein-coupled receptors to mediate phototransduction [3]. RA binds to ligand-activated transcription factors of the nuclear hormone receptor superfamily and controls processes as diverse as cell differentiation, embryonic development, immunity, and metabolism [4-6].

β-Carotene-rich fruits and vegetables also contain a whole series of long-chain (>C20) apocarotenoids [7-9]. These lipids are structurally related to retinoids and derive by chemical and enzymatic oxidative cleavage of double bonds in the polyene carbon backbone of β-carotene and other carotenoids [10, 11]. β-Apocarotenoids are also used as food colorants and their concentration is enriched in genetically engineered carotenoid-rich crops [12, 13].

Emerging evidence indicates that β-apocarotenoids compete with endogenous retinoids for binding proteins and metabolizing enzymes [14]. In this process, the end group of a β-apocarotenoid can be converted to the corresponding alcohol, aldehyde, and carboxylic acid or esterified with acyl groups [15-17]. Specific apocarotenoids can bind to nuclear hormone receptors and modulate their activities, including the peroxisome proliferator activated receptors (PPARs), retinoic acid receptors (RAR), and retinoid X receptors (RXR) [7, 8, 18, 19]. Moreover, apocarotenoids have been implicated as modulators of mitochondrial function [20], in various aspects of cancer biology [21, 22], and in lipoprotein metabolism at the placental-

fetal barrier [23, 24]. However, little is known about the metabolism of these lipids including its homeostatic control.

The enzyme family of carotenoid cleavage oxygenases (CCOs) catalyze the oxidative cleavage and isomerization of double bonds of polyunsaturated organic compounds, including stilbenes and carotenoids [25]. In mammals, the enzymes' roles in carotenoid metabolism and vitamin A synthesis have been well established [26]. Recently, CCOs have been implicated in metabolism of apocarotenoids. β-carotene-oxygenase-1 (BCO1) converts long chain β-apocarotenoids into all-*trans*-retinal (vitamin A aldehyde) by oxidation at position C15,C15' of the polyene chain [15, 27, 28]. The physiological relevance of this pathway has been demonstrated in mice [29, 30], indicating that long-chain β-apocarotenoids are provitamins on their own right.

The β-carotene-oxygenase-2 (BCO2) is another mammalian member of the CCO protein family of non-heme iron oxygenases [31]. BCO2 is a mitochondrial protein and catalyzes oxidative cleavage of carotenoids at position C9,C10 [31-33], BCO2 is expressed in several tissues in humans and rodents [31, 34] and displays broad substrate specificity for various carotenoids [30, 32, 35-38]. BCO2 converts carotenoids eccentrically into an ionone and a long chain apocarotenoid [15, 17]. However, there are conflicting reports in the literature whether BCO2 engages in apocarotenoid metabolism and maintains the homeostasis of these compounds in mammalian tissues [30, 36, 38]. Therefore, we here aimed at elucidating the role of BCO2 in β-apocarotenoid metabolism using biochemical and genetic approaches.

RESULTS AND DISCUSSION

Animals, including humans can absorb β-apocarotenoids from the food matrix or produce them from dietary carotenoid precursor molecules [9]. Apocarotenoids recently attained general scientific interest because of their putative physiological functions in vertebrate biology [14]. This poses the question how mammals can accurately, efficiently, and effectively metabolize these natural compounds and maintain their homeostasis. In this work, we show that the mammalian enzyme BCO2 can cope with this metabolic challenge. We elucidate the structural and biochemical basis of substrate binding and double bond cleavage by the enzyme. Evidence from genetic studies in mice indicate that BCO2 engages in apocarotenoid metabolism and maintains homeostatic levels of these compounds.

BCO2 converts the alcohol, aldehyde, and carboxylic acid form of a β-apocarotenoid

A robust and reliable protein expression system is required to yield an adequate amount of properly folded and enzymatically active protein. We established protocols to express BCO2 cDNA fused with a *malE* gene encoding maltose-binding protein (MBP) in *E. coli* [39]. We used affinity chromatography to purify the murine MBP-BCO2 fusion protein (mBCO2) (Fig. 1a).

β-Apocartenoids consist of a β-ionone ring, a polyene chain, and a polar end group. The end group can exist as alcohol, carbonyl, and carboxylic acid. We first tested whether the oxidation state of the end group affected the turnover of a given apocarotenoid by mBCO2. In this experiment, β-apo-10'-carotenol, β-apo-10'-carotenal, and β-apo-10'-carotenoic acid

were respectively used as alcohol, aldehyde, and carboxylic acid substrates (Fig. 1b). Kinetic analysis revealed the highest turnover rate of the enzyme for β-apo-10' carotenol, followed by β -apo-10'-carotenal, and β-apo-10' carotenoic acid under the applied conditions (Fig. 1c). After the enzyme assays, substrates and products were extracted and separated by HPLC and diapocarotenoid cleavage products became detectable (Fig. 1d-f).

BCO2 converts β-apocarotenoids with variable chain length

We next analyzed whether the length of the polyene chain of a β-apocarotenoid affected the enzymatic turnover by mBCO2. Thus, we performed tests with β-apo-4'-carotenoic acid (C34), β-apo-6'-carotenoic acid (C32), β-apo-8'-carotenoic acid (C30), β-apo-10'-carotenoic acid (C27), β-apo-12'-carotenoic acid (C25), and β-apo-14'-carotenoic acid (C22) (Fig. 2a). Notably, β-apo-4'-carotenoic acid possesses a polyene chain that is longer than in a bicyclic C40 carotenoid (Fig. 2a). After the assays, we analyzed the occurrence of products by HPLC (Fig. 2 b-d). We were able to capture the cleavage products of β-apo-4'-carotenoic acid, β-apo-6'-carotenoic acid, β-apo-8'-carotenoic acid, and β-apo-10' carotenoic acid (Fig.S1). UV-visible absorption spectra of products revealed that the polyene chain length was shortened as indicated by a bathochromic absorbance shift and a prolonged retention time caused by the increase in polarity (Fig. 2 c,d). We did not detect the diapocarotenoid cleavage products for the β-apo-12'-carotenoic acid and for β-apo-14'-carotenoic acid reactions but observed a decrease of the substrate peaks in the assays. The failure to detect the products of the reaction is most likely caused by their polarity, which impedes the extraction of the compounds into the organic solvent during sample preparation for HPLC analysis.

Cleavage of apocarotenoids with modified rings

Apocarotenoids with hydroxylated β-ionone rings derive from chemical and enzymatic processing of xanthophyll and exist in human blood [40]. Previously, we showed that mouse BCO2 can cleave 3-hydroxy-β-apo-8'-carotenal [30] and 3-hydroxy-β-apo-12'–carotenal with a two double bonds shorter polyene chromophore [39]. We now wondered whether mBCO2 can convert 3-hydroxy-retinal which is also known as vitamin A_3-aldehyde. We produced 3-hydroxy-retinal with the help of an apocarotenoid oxygenase ACO from *Synechocystis* [41]. For this experiment, we first incubated 3-hydroxy-β-apo-12'-carotenal with the bacterial ACO to produce 3-hydroxy-retinal. Then we added mBCO2 protein to the reaction mixture to test whether 3-hydroxy-retinal was further converted by mBCO2 (Fig 3a). Substrates and products of the different reactions were separated by HPLC and characterized by their retention time and spectral characteristics. The HPLC traces showed that incubation with ACO alone resulted in 3-hydroxy-retinal production as indicated by the increased retention time and spectral properties of this compound (Fig. 3b,c). Subsequent addition of mBCO2 to the mixture resulted in a decrease of 3-hydroxy-retinal product (Fig. 3b). Additionally, mBCO2 also converted the remaining 3-hydroxy-β-apo-12'-carotenal substrate from the first incubation step into the corresponding diapocarotene product.

Ionone ring site modifications at position 4 are found in natural carotenoids and apocartenoids. To test whether BCO2 can convert substrates with ketolated ionone rings, we incubated canthaxanthin (β,β-carotene-4,4'-dione) in the presence of mBCO2. Isolation of

the reaction products and subsequent HPLC analysis revealed that mBCO2 converted this carotenoid by successive removal of the ketolated rings into a diapcarotenoid product. (Fig. S2). Taken together, our enzyme assays revealed that recombinant mBCO2 converted apocarotenoids with different chain length (C20 to C40) and β-ring modifications into diapocarotenoid products. These enzymatic properties allow BCO2 the processing of a whole panoply of naturally occurring β-apocarotenoids. Our recent characterization of human BCO2 indicates that the enzyme's function in apocarotenoid metabolism is well conserved [39]. Surprisingly, studies by others came to the conclusion that the closely related chicken and ferret BCO2s do not convert apocarotenoids [36, 38]. We cannot rule out that BCO2 from different species display variability in substrate specificity. However, evolutionary conservation of amino acids in the substrate binding cleft as well as the overall conserved fold of BCO2s rather suggest that the observed discrepancy is related to experimental conditions. Protein misfolding and aggregation were reported for recombinant BCO2, particularly when the enzyme is expressed as a pre-protein with its mitochondrial leader sequence [39, 42]. Moreover, the diapocarotenoid reaction products are chemically instable and difficult to detect when present in small amounts. Thus, it might be worthwhile in future studies to express and compare BCO2s from different vertebrate species under the improved assay conditions that we used in this study.

BCO2 reaction follows a dioxygenase reaction mechanism

A dioxygenase reaction mechanism has been reported for canonical double bond cleaving CCOs, including plant CCD1, bacterial ACO, fungal NOV2, insect NinaB, and human BCO1 [27, 43-45]. To clarify how the BCO2 enzymatic conversion of apocarotenoids proceeds, we conducted heavy isotope labeling experiments in $^{18}O_2$ saturated reaction buffer. We used 3-hydroxy-β-12-carotenal as substrate and monitored the reaction by determining isotope incorporation into the 3-hydroxy-β-ionone product by LC-MS (Fig. 4). The measurement of 3-hydroxy-β-ionone brought the advantage that there is no oxygen exchange between the labeled ketone-group of the reaction product and bulk water. This exchange rapidly occurs with aldehyde groups of apocarotenal products via an apocarotene-diol intermediate and chicken BCO1 was erroneously characterized as monoxygenase in a previous study [43]. In our assays, the percentage of ^{18}O incorporation into the product, as determined by the ratio of the signal intensities for non-labelled ^{16}O-3-hydroxy-ionone (m/z of 209, $[MH]^+$) and the ^{18}O-labelled 3-hydroxy-β-ionone at m/z = 211, $[MH]^+$, was 68.4% with a standard deviation of 0.71 in repeated experiments (Fig. 4a, b). A mono-oxygenase reaction would maximally lead to a labeling of 50% of the heavy isotopologue. The theoretical maximum incorporation of molecular ^{18}O in a dioxygenase reaction mechanism can reach 100%. A complete labeling of the reaction product was likely prevented by an incomplete degassing of the buffer or enzyme bound oxygen. We failed to detect the molecular mass of dialdehyde reaction product. The main issue with this failure was its limited amounts as well as its reactivity with other components of the reaction mixture. However, the high exchange rate between the dialdehyde groups of the diapocarotenoid and bulk water would likely have rendered isotopic mixtures, which are difficult to interpret. Thus, we propose based on the incorporation rate of ^{18}O into 3-hydroxy-β-ionone that the BCO2 reaction follows a dioxygenase reaction mechanism as it has been previously demonstrated for other members of the CCO family [27, 43-45].

How do carotenoids and apo carotenoids bind to BCO2?

The entrance of the substrate tunnel of the vitamin A forming enzyme BCO1 is selective for non-substituted β-ionone ring sites [30]. The substrate promiscuity of BCO2 asks for a wider substrate tunnel that can detect the scissile C9,C10 bond in assorted carotenoids and apocarotenoids substrates. To understand the spatial arrangement between BCO2 and its substrates, we produced a homology model for BCO2 using the structure of the archaeal CCO from Candidatus Nitrosotalea devanaterra (NdCCD) [46]. The root-mean-square deviation for the structural alignment between mBCO2 and NdCCD was 1.1 Å (Fig. S3). We modeled a carotenoid substrate into the binding cavity of the predicted mBCO2 structure (Fig. 5a). The model indicated that the lining of the substrate-binding cavity is mainly made from hydrophobic residues (Fig. 5a). Sequence comparison revealed that most of the amino acid residues in the substrate tunnel were conserved between BCO1 and BCO2 (Fig. S4a). However, we identified amino acid residues, which differed between BCO1 and BCO2 and which may contribute to the regioselectivity of double bond cleavage. These amino acids included Phe102, Asn132, and Phe525, which are highly conserved between BCO2s from different species (Fig. S4a,b). We first focused on Phe102 and Phe525, which interacted with the central polyene chain of the substrate in our model (Fig. 5a). To address the role of these aromatic side residues, we mutated Phe525 and Phe102 into leucine residues to establish single and double mutant variants. We expressed different mBCO2 variants and performed enzyme assays with carotenoid and apocarotenoid substrates. As controls, we included maltose binding protein and wild type mBCO2 in our assays. The F102L single mutant and the wild type mBCO2 converted meso-zeaxanthin into 10’,10-apocarotene-dialdehyde by the removal of both ionone ring sites of the bicyclic carotenoid substrate (Fig. 5b,d). The wild type and F102L mutant variant also converted 3-hydroxy-apo-12’-carotenal into the corresponding 12’,10-diapocarotene-dialdehyde product (Fig. 5c,d). By contrast, the F525L single mutant and the F525L/F102L double mutant variants converted meso-zeaxanthin into 3-hydroxy-β-apo-10’-carotenal by the removal of only one ionone ring site (Fig. 5b,d). Accordingly, these mutant variants did not convert the apocarotenal substrate into the corresponding diapocarotene-dialdehyde product (Figure 5c).

We next focused on the amino acid Asn132. This residue is predicted to be involved in the hydrogen bonding network that stabilizes the loop on top of the cleavage site of a carotenoid substrate (Fig. 5a and Fig. S3b). We mutated Asn132 into Leu, which is the amino acid in the corresponding position of BCO1. We also mutated Asn132 into Arg with a bulkier and positively charged side chain. We observed that the N132L mutant variant displayed a lower conversion of the meso-zeaxanthin substrate when compared to wild type mBCO2 (Fig. 6a,c). Additionally, both the 3-hydroxy-β-apo-10’-carotenal and the 10’,10-apocarotene-dialdehyde product became detectable whereas the wild type mBCO2 produced the dialdehyde as the major product under the applied experimental conditions (Fig. 6a,c). In contrast, the N132L mutant variant and the wild type mBCO2 readily converted the apocarotenoid substrate into a dialdehyde product (Fig. 6b,c). The N132R mBCO2 mutant variant, with bulky amino acid substitution, displayed no activity with the carotenoid and apocarotenoid substrates (Fig. 6a,b). Western blot analysis with the different mBCO2 mutant variants demonstrated that all recombinant proteins were expressed in soluble form (Fig.

S5), indicating that the lack of enzymatic activity was not caused by misfolding and aggregation of the mutant BCO2 proteins.

Together, our structural analyses indicated that BCO2 displayed a bipartite substrate-binding cavity that can discriminate between carotenoids and apocarotenoids. The outcome of the studies best fits a model in which the cleavage of a carotenoid substrate occurs in a two-step mechanism as outlined in the cartoon illustration in Fig. 7. The initial binding of the carotenoid involves amino acid Asn132. A N132L variant of BCO2 displayed reduced conversion of carotenoid substrate into apocarotenoid and diapocarotenoid products (Fig. 6a,c). By contrast, an apocarotenoid substrate was readily converted by the N132L variant (Fig. 6b,c). Asn132 likely stabilizes the π-stacking interactions in the conserved HWF motif in the substrate-binding cavity (Fig. 5a and Fig. S4). Substitution of Asn132 by a bulky Arg residue completely abolished enzymatic activity of the mutant enzyme (Fig. 6a,b). In the second step, the phenyl ring of Phe525 plays a crucial role in positioning the apocarotenoid to the active center (Fig. 5a). Evidence for this assumption was obtained in a F525L variant of the BCO2 enzyme. The mutant variant failed to catalyze a sequential cleavage at double bonds C9,C10 and C9',C10' of a bicyclic carotenoid substrate (Fig. 5b). In accordance with this observation, the F525L variant failed to cleave an apocarotenoid substrate (Fig. 5c). Thus, mBCO2 specifically interacted with the polyene chains of their substrates. The structurally more variable ionone rings did not contribute to this interaction, thereby explaining the substrate promiscuity of the enzyme.

BCO2 contributes to apocarotenoid metabolism in mice

Finally, we analyzed in mice whether BCO2 enzyme engages in β-apocarotenoid metabolism. To address this question, we used a genetic approach and supplemented wild type, *Bco1*$^{-/-}$, and *Bco2*$^{-/-}$ mice with β-10'-apocarotenal and 3-hydroxy-β-apo-12'carotenal by oral gavage. After the gavage, we sacrificed animals and extracted lipids from the liver. We observed that 3-hydroxy-β-apo-12'carotenal became detectable in lipid extracts of liver of BCO2-deficient mice (Fig. 8a). The substance was absent in wild type and *Bco1*$^{-/-}$ mice, indicating that the accumulation depended on the *Bco2* genotype. Additionally, we detected two compounds with a slightly shorter retention time and a slightly longer retention time with spectral characteristic of carotenoids (Fig. 8a).

β-apo-10'-carotenal accumulated independent of the genotype in the liver of all mice. The major metabolite was β-apo-10'-carotenol (Fig. 8b). We identified β-apo-10'-carotenol by its spectral characteristics and retention time as compared to an authentic standard (Fig. S6). The highest amount of β-apo-10'-carotenol was found in BCO2-deficient mouse liver extract, the lowest concentration in wild type mouse liver extract. Again, we detected the two compounds resembling carotenoids in lipid extracts of *Bco2*$^{-/-}$ mice (Fig 8b). We determined the molecular mass of these compounds as 532.66 m/z. Since both compounds also became detectable in non-gavaged *Bco2*$^{-/-}$ control mice (Fig. S7), we concluded that they represent metabolites of ingredients of chow rather than metabolites of the supplemented β-apocarotenoids. In fact, the chow contained significant amount of lutein (Fig. S8). From this observation, we inferred that the unknown compounds most likely is a

metabolite of lutein. Indeed, other and we previously showed that the hydroxylated β- and ε-ionone rings of lutein are chemically modified in mice [32, 47].

In conclusion, apocarotenoids have emerged as novel class of biologically active molecules in vertebrates [14]. Our study provided biochemical and structural insights into the enzymatic processing of these lipids and demonstrate that BCO2 is an important player in path. A better understanding of the biochemical mechanisms that control apocarotenoid homeostasis and function will aid in the development of nutritional intervention strategies to improve health and longevity in the general population.

METHODS

Materials

All chemicals, unless otherwise stated, were purchased from Fisher and Sigma Aldrich. Carotenoids and apocarotenoids were a gift from Dr. Adrian Wyss (DSM, Sisseln, Switzerland). Plasmid and RNA isolation kits were purchased from Qiagen.

Mouse strains and husbandry

Animal procedures and experiments were approved by the Case Western Reserve University Institutional Animal Care and Use Committee and conformed to recommendations of both the American Veterinary Medical Association Panel on Euthanasia and the ARVO Statement for the Use of Animals in Ophthalmic and Vision Research. Wild type (WT), *Bco1*$^{-/-}$ [48] and *Bco2*$^{-/-}$ [49] mice were bred and raised on standard mouse chow. At 2 month of age male mice (n = 3 per genotype) were gavaged with β-apo-10′-carotenal or 3-hydroxy-β-apo-12’-carotenal prepared in sesame oil (0.5 mg per mouse) in the morning. After 24 hours, mice were gavaged again in the early morning and sacrificed after 4 hours. Livers were dissected and stored at −80°C until further analysis.

Protein expression and purification

Murine *Bco2* cDNA was cloned in pMAL expression vector (New England Biolabs) and expressed in *E. coli* BL21 (DE3) strain as maltose binding protein fusion protein (mBCO2). Protein expression and purification was conducted as previously described [39]. Maltose binding protein (MBP) was expressed and purified by the same protocol. The apocarotenoid oxygenase from Synechocystis was expressed in *E. coli* and purified by established protocols [41]. SDS-PAGE was used to analyze the purity of the proteins. Protein fractions were combined and concentrated using centrifugal units (Millipore).

Modeling of protein structures

Swiss modeling was used to build a homology model for the different BCO2 enzymes [50] based on the orientation of carotenoid substrate in the structure of the *Candidatus Nitrosotalea devanaterra* CCD (NdCCD) (PDB accession number 6VCH) [46]. Then, carotenoid and apocarotenoids were modelled into the active site cavity using Coot software [51] . Pymol software was used to align structures and to create figures.

Site directed mutagenesis

Quick change site directed mutagenesis kit (Agilent) was used to mutate mBCO2 F102L, N132L, N132R and F525L residues. mBCO2 cDNA cloned in pMAL vector was used as the template for the mutations. Mutation primers were the following: mBCO2 F102L forward primer, 5'GGCCAGCGTGCCTAATTCTGAGATCACAATTCTACC3' reverse primer 5'GGTAGAATTGTGATCTCAGAATTAGGCACGCTGGCC3'; mBCO2 N132R forward primer, 5'TGCACAAAGTTGACTCGGGTGTTGTCAGTC3' reverse primer 5'GACTGACAACACCCGAGTCAACTTTGTGCA3'; mBCO2 R132L forward primer 5'TGCACAAAGTTGACTAGGGTGTTGTCAGTCA3' reverse primer 5'TGACTGACAACACCCTAGTCAACTTTGTGCA3'; mBCO2 F525L forward primer, 5'CAAAGGTGCCATGTAACCCGTAAGGCA3' reverse primer 5'TGCCTTACGGGTTACATGGCACCTTTG3'.

Enzyme activity assay

β-Apocarotenoids (2000 pmol) were dissolved in acetone and were mixed with 100 μL reaction buffer (20 mM Tricine, 150 mM NaCl, 0.5 mM TCEP, 0.2% v/v Triton x-100 at pH 7.4). Carotenoids (2000 pmol) were dissolved in acetone and mixed with 3% w/v DMN in 100% ethanol. The solvent was evaporated with dry vacuum centrifugation (Eppendorf). The carotenoid detergent mixture was dissolved with 50 μL of reaction buffer (20 mM Tricine, 150 mM NaCl, 0.5 mM TCEP at pH 7.4). 50 μL of enzyme solution (50 μg) was added to apocarotenoid and carotenoid solution and the mixture was incubated at 37 °C under shaking at 600 rpm in a thermomixer (Eppendorf) for 10 minutes. The reactions were stopped by the addition of 100 μL of 10% acetic acid in water (v/v), 400 μL of acetone, 400 μL of diethyl ether and 100 μL of petroleum ether. Organic and aqueous layers were separated with a 10 sec spin at 3000 x g. The organic layer was collected and evaporated in a dry vacuum centrifuge (Eppendorf). β-Apo-carotenoic acids were dissolved in HPLC solvent 1 (hexanes: ethyl acetate, 80:20 (v/v)) with 12.5 μL acetic acid per 100 mL), β-Apo-carotenals, β-apo-carotenols, and carotenoids were dissolved in solvent 2 (hexane: Ethyl acetate, 80:20, (v/v) and solvent 3 (hexane: Ethyl acetate, 70:30, (v/v) depending on their polarity. HPLC analyses were carried out on an Agilent 1260 Infinity Quaternary HPLC system (Santa Clara, CA, USA) equipped with a pump (G1312C) with an integrated degasser (G1322A), a thermostated column compartment (G1316A), an auto sampler (G1329B), a diode-array detector (G1315D), and online analysis software (Chemstation). The analyses were carried out at 25°C using a normal-phase Zorbax Sil (5 μm, 4.6 x 150 mm) column (Agilent Technologies, Santa Clara, CA) protected with a guard column with the same stationary phase. Chromatographic separation was achieved by isocratic flow at 1.4 mL per minute.

Enzyme kinetics

β-Apo-10'-carotenal, β-apo-10'-carotenol and β-apo-10'-carotenoic acid (12 μM final concentration) were dissolved in acetone and mixed with reaction buffer (20 mM Tricine, 150 mM NaCl, 0.5 mM TCEP 0.2% Triton x-100 at pH 7.4). Then 50 μg of enzyme was added to the reaction mixture. The progress of the reaction was monitored by determining the decrease in absorbance of the substrate over time (β-Apo-10'-carotenal and β-apo-10'-

carotenoic acid at 420nm, β-apo-10'-carotenol at 400 nm) . Values were detemined with the help of calibration curve created with known amounts of authentic standard substances.

HPLC analysis of mouse chow

The ground chow diet (350 mg) was incubated with 800 μL of acetone overnight at room temperature. The next day, 400 μL of acetone separated from the mixture, and carotenoids were extracted with 100 μL of water, 400 μL of diethyl ether, and 100 μL of petroleum ether. The organic layer was separated and evaporated by dry vacuum centrifugation. The debris was dissolved in HPLC solvent 3 (hexane: ethyl acetate, 70:30, (v/v)) and subjected to HPLC analysis with HPLC solvent 3 with a flow rate of 1.4 mL per minute.

Isotope labelling experiments

Labeling experiments with $^{18}O_2$ were performed in 10-mL screw-capped glass vials with a gas-tight Teflon septum. All volumes in the preparation of substrate micelles were increased 5-fold and dried accordingly in the glass vial and kept on ice. Inert gas saturation cycles prior to saturation with $^{18}O_2$ mBCO2 solution was added to the glass vial and the buffer was degassed and deoxygenated by applying vacuum degassing for several times. Then, the mixture was saturated with $^{18}O_2$ by aerating the solution on ice for 1 min with a release syringe placed into the septum. Then, after removal of the release syringe, the solution was saturated with$^{18}O_2$ once more for 2 min. The sample was vortexed and incubated at 22°C for 4 min. The enzymatic reactions were stopped by adding acetone and diethyl ether, and petroleum ether as described above. Isotopic composition of 3-hydroxy-β-ionone resulting from BCO2 activity was analyzed by LC/MS. For this purpose, the organic extract of the reaction mixture was dried down in a SpeedVac, resuspended in 100 μL of acetonitrile, and injected onto a Phenomenex Gemini C18 column (250 x 4.6 mm) coupled to Agilent 1100 HPLC system and LTQ Velos ion-trap mass spectrometer (Thermo Scientific). 3-hydroxy-β-ionone was eluted in the gradient of acetonitrile in water (30% - 100%) developed over 20 minutes at flow rate of 0.7 mL/min. The eluent was directed into an electrospray ionization probe (Thermo Scientific) working in positive mode. LC/MS data were collected and analyzed using Thermo Xcalibur software version 2.1.0.1139.

Supplementary Material

Refer to Web version on PubMed Central for supplementary material.

Acknowledgments

We wish to thank A. Wyss (DSM) for the gift of 3-hydroxy-β-12'-apo-carotenal and zeaxanthin enantiomers. We are grateful to H. Ernst (BASF) for the gift of the different β-apocarotenoic acids.

Funding and additional information

The research was supported by grants from the National Eye Institute (EY020551, EY028121, EY007157 to J.V.L., and EY023948 to M.G.) and P30 Core grant EY011373 as well as the Department of Veterans Affairs (I01BX004939 to P.D.K.). The content is solely the responsibility of the authors and does not necessarily represent the official views of the National Institutes of Health.

References

[1]. Kiser PD, Golczak M, and Palczewski K (2014) Chemistry of the retinoid (visual) cycle, Chemical reviews 114, 194–232. [PubMed: 23905688]

[2]. Kedishvili NY (2013) Enzymology of retinoic acid biosynthesis and degradation, J Lipid Res 54, 1744–1760. [PubMed: 23630397]

[3]. Arshavsky VY, Lamb TD, and Pugh EN Jr. (2002) G proteins and phototransduction, Annu Rev Physiol 64, 153–187. [PubMed: 11826267]

[4]. Rhinn M, and Dollé P (2012) Retinoic acid signalling during development, Development (Cambridge, England) 139, 843–858.

[5]. Hall JA, Grainger JR, Spencer SP, and Belkaid Y (2011) The role of retinoic acid in tolerance and immunity, Immunity 35, 13–22. [PubMed: 21777796]

[6]. Blaner WS (2019) Vitamin A signaling and homeostasis in obesity, diabetes, and metabolic disorders, Pharmacol Ther 197, 153–178. [PubMed: 30703416]

[7]. Eroglu A, Hruszkewycz DP, Curley RW Jr., and Harrison EH (2010) The eccentric cleavage product of beta-carotene, beta-apo-13-carotenone, functions as an antagonist of RXRalpha, Arch Biochem Biophys 504, 11–16. [PubMed: 20678466]

[8]. Eroglu A, Hruszkewycz DP, dela Sena C, Narayanasamy S, Riedl KM, Kopec RE, Schwartz SJ, Curley RW Jr., and Harrison EH (2012) Naturally occurring eccentric cleavage products of provitamin A beta-carotene function as antagonists of retinoic acid receptors, J Biol Chem 287, 15886–15895. [PubMed: 22418437]

[9]. Harrison EH, dela Sena C, Eroglu A, and Fleshman MK (2012) The formation, occurrence, and function of beta-apocarotenoids: beta-carotene metabolites that may modulate nuclear receptor signaling, Am J Clin Nutr 96, 1189S–1192S. [PubMed: 23053561]

[10]. Auldridge ME, McCarty DR, and Klee HJ (2006) Plant carotenoid cleavage oxygenases and their apocarotenoid products, Curr Opin Plant Biol 9, 315–321. [PubMed: 16616608]

[11]. Wang XD, Tang GW, Fox JG, Krinsky NI, and Russell RM (1991) Enzymatic conversion of beta-carotene into beta-apo-carotenals and retinoids by human, monkey, ferret, and rat tissues, Arch Biochem Biophys 285, 8–16. [PubMed: 1899329]

[12]. Zheng X, Giuliano G, and Al-Babili S (2020) Carotenoid biofortification in crop plants: citius, altius, fortius, Biochim Biophys Acta Mol Cell Biol Lipids 1865, 158664. [PubMed: 32068105]

[13]. Ilg A, Yu Q, Schaub P, Beyer P, and Al-Babili S (2010) Overexpression of the rice carotenoid cleavage dioxygenase 1 gene in Golden Rice endosperm suggests apocarotenoids as substrates in planta, Planta 232, 691–699. [PubMed: 20549230]

[14]. Harrison EH, and Quadro L (2018) Apocarotenoids: Emerging Roles in Mammals, Annu Rev Nutr 38, 153–172. [PubMed: 29751734]

[15]. Amengual J, Widjaja-Adhi MA, Rodriguez-Santiago S, Hessel S, Golczak M, Palczewski K, and von Lintig J (2013) Two carotenoid oxygenases contribute to mammalian provitamin A metabolism, J Biol Chem 288, 34081–34096. [PubMed: 24106281]

[16]. Durojaye BO, Riedl KM, Curley RW Jr., and Harrison EH (2019) Uptake and metabolism of beta-apo-8'-carotenal, beta-apo-10'-carotenal, and beta-apo-13-carotenone in Caco-2 cells, J Lipid Res 60, 1121–1135. [PubMed: 30846527]

[17]. Amengual J, Gouranton E, van Helden YG, Hessel S, Ribot J, Kramer E, Kiec-Wilk B, Razny U, Lietz G, Wyss A, Dembinska-Kiec A, Palou A, Keijer J, Landrier JF, Bonet ML, and von Lintig J (2011) Beta-Carotene Reduces Body Adiposity of Mice via BCMO1, PloS one 6, e20644. [PubMed: 21673813]

[18]. Ziouzenkova O, Orasanu G, Sukhova G, Lau E, Berger JP, Tang G, Krinsky NI, Dolnikowski GG, and Plutzky J (2007) Asymmetric cleavage of beta-carotene yields a transcriptional repressor of retinoid X receptor and peroxisome proliferator-activated receptor responses, Mol Endocrinol 21, 77–88. [PubMed: 17008383]

[19]. Eroglu A, and Harrison EH (2013) Carotenoid metabolism in mammals, including man: formation, occurrence, and function of apocarotenoids, J Lipid Res 54, 1719–1730. [PubMed: 23667178]

[20]. Siems W, Sommerburg O, Schild L, Augustin W, Langhans CD, and Wiswedel I (2002) Beta-carotene cleavage products induce oxidative stress in vitro by impairing mitochondrial respiration, FASEB J 16, 1289–1291. [PubMed: 12154001]

[21]. Lim JY, and Wang XD (2020) Mechanistic understanding of beta-cryptoxanthin and lycopene in cancer prevention in animal models, Biochim Biophys Acta Mol Cell Biol Lipids 1865, 158652. [PubMed: 32035228]

[22]. Liu C, Wang XD, Bronson RT, Smith DE, Krinsky NI, and Russell RM (2000) Effects of physiological versus pharmacological beta-carotene supplementation on cell proliferation and histopathological changes in the lungs of cigarette smoke-exposed ferrets, Carcinogenesis 21, 2245–2253. [PubMed: 11133814]

[23]. Costabile BK, Kim YK, Iqbal J, Zuccaro MV, Wassef L, Narayanasamy S, Curley RW Jr., Harrison EH, Hussain MM, and Quadro L (2016) beta-Apo-10'-carotenoids Modulate Placental Microsomal Triglyceride Transfer Protein Expression and Function to Optimize Transport of Intact beta-Carotene to the Embryo, J Biol Chem 291, 18525–18535. [PubMed: 27402843]

[24]. Quadro L, Giordano E, Costabile BK, Nargis T, Iqbal J, Kim Y, Wassef L, and Hussain MM (2020) Interplay between beta-carotene and lipoprotein metabolism at the maternal-fetal barrier, Biochim Biophys Acta Mol Cell Biol Lipids 1865, 158591. [PubMed: 31863969]

[25]. Daruwalla A, and Kiser PD (2020) Structural and mechanistic aspects of carotenoid cleavage dioxygenases (CCDs), Biochim Biophys Acta Mol Cell Biol Lipids 1865, 158590. [PubMed: 31874225]

[26]. von Lintig J, Moon J, and Babino D (2021) Molecular components affecting ocular carotenoid and retinoid homeostasis, Prog Retin Eye Res 80, 100864. [PubMed: 32339666]

[27]. Dela Sena C, Riedl KM, Narayanasamy S, Curley RW Jr., Schwartz SJ, and Harrison EH (2014) The human enzyme that converts dietary provitamin a carotenoids to vitamin a is a dioxygenase, J Biol Chem 289, 13661–13666. [PubMed: 24668807]

[28]. Sharma RV, Mathur SN, and Ganguly J (1976) Studies on the relative biopotencies and intestinal absorption of different apo-beta-carotenoids in rats and chickens, Biochem J 158, 377–383. [PubMed: 985434]

[29]. Spiegler E, Kim YK, Hoyos B, Narayanasamy S, Jiang H, Savio N, Curley RW Jr., Harrison EH, Hammerling U, and Quadro L (2018) beta-apo-10'-carotenoids support normal embryonic development during vitamin A deficiency, Scientific reports 8, 8834. [PubMed: 29892071]

[30]. Kelly ME, Ramkumar S, Sun W, Colon Ortiz C, Kiser PD, Golczak M, and von Lintig J (2018) The Biochemical Basis of Vitamin A Production from the Asymmetric Carotenoid beta-Cryptoxanthin, ACS Chem Biol 13, 2121–2129. [PubMed: 29883100]

[31]. Kiefer C, Hessel S, Lampert JM, Vogt K, Lederer MO, Breithaupt DE, and von Lintig J (2001) Identification and characterization of a mammalian enzyme catalyzing the asymmetric oxidative cleavage of provitamin A, J Biol Chem 276, 14110–14116. [PubMed: 11278918]

[32]. Amengual J, Lobo GP, Golczak M, Li HN, Klimova T, Hoppel CL, Wyss A, Palczewski K, and von Lintig J (2011) A mitochondrial enzyme degrades carotenoids and protects against oxidative stress, FASEB J 25, 948–959. [PubMed: 21106934]

[33]. Palczewski G, Amengual J, Hoppel CL, and von Lintig J (2014) Evidence for compartmentalization of mammalian carotenoid metabolism, FASEB J 28, 4457–4469. [PubMed: 25002123]

[34]. Lindqvist A, He YG, and Andersson S (2005) Cell type-specific expression of beta-carotene 9',10'-monooxygenase in human tissues, J Histochem Cytochem 53, 1403–1412. [PubMed: 15983114]

[35]. Hu KQ, Liu C, Ernst H, Krinsky NI, Russell RM, and Wang XD (2006) The biochemical characterization of ferret carotene-9',10'-monooxygenase catalyzing cleavage of carotenoids in vitro and in vivo, J Biol Chem 281, 19327–19338. [PubMed: 16672231]

[36]. Mein JR, Dolnikowski GG, Ernst H, Russell RM, and Wang XD (2010) Enzymatic formation of apo-carotenoids from the xanthophyll carotenoids lutein, zeaxanthin and beta-cryptoxanthin by ferret carotene-9',10'-monooxygenase, Arch Biochem Biophys 506, 109–121. [PubMed: 21081106]

[37]. Lobo GP, Isken A, Hoff S, Babino D, and von Lintig J (2012) BCDO2 acts as a carotenoid scavenger and gatekeeper for the mitochondrial apoptotic pathway, Development 139, 2966–2977. [PubMed: 22764054]

[38]. Dela Sena C, Sun J, Narayanasamy S, Riedl KM, Yuan Y, Curley RW Jr., Schwartz SJ, and Harrison EH (2016) Substrate Specificity of Purified Recombinant Chicken beta-Carotene 9',10'-Oxygenase (BCO2), J Biol Chem 291, 14609–14619. [PubMed: 27143479]

[39]. Thomas LD, Bandara S, Parmar VM, Srinivasagan R, Khadka N, Golczak M, Kiser PD, and von Lintig J (2020) The human mitochondrial enzyme BCO2 exhibits catalytic activity toward carotenoids and apocarotenoids, J Biol Chem 295, 15553–15565. [PubMed: 32873706]

[40]. Giuffrida D, Donato P, Dugo P, and Mondello L (2018) Recent Analytical Techniques Advances in the Carotenoids and Their Derivatives Determination in Various Matrixes, J Agric Food Chem 66, 3302–3307. [PubMed: 29533609]

[41]. Sui X, Kiser PD, Che T, Carey PR, Golczak M, Shi W, von Lintig J, and Palczewski K (2014) Analysis of Carotenoid Isomerase Activity in a Prototypical Carotenoid Cleavage Enzyme, Apocarotenoid Oxygenase (ACO), J Biol Chem 289, 12286–12299. [PubMed: 24648526]

[42]. Babino D, Palczewski G, Widjaja-Adhi MA, Kiser PD, Golczak M, and von Lintig J (2015) Characterization of the Role of beta-Carotene 9,10-Dioxygenase in Macular Pigment Metabolism, J Biol Chem 290, 24844–24857. [PubMed: 26307071]

[43]. Schmidt H, Kurtzer R, Eisenreich W, and Schwab W (2006) The carotenase AtCCD1 from Arabidopsis thaliana is a dioxygenase, J Biol Chem 281, 9845–9851. [PubMed: 16459333]

[44]. Sui X, Golczak M, Zhang J, Kleinberg KA, von Lintig J, Palczewski K, and Kiser PD (2015) Utilization of Dioxygen by Carotenoid Cleavage Oxygenases, J Biol Chem 290, 30212–30223. [PubMed: 26499794]

[45]. Babino D, Golczak M, Kiser PD, Wyss A, Palczewski K, and von Lintig J (2016) The Biochemical Basis of Vitamin A3 Production in Arthropod Vision, ACS Chem Biol 11, 1049–1057. [PubMed: 26811964]

[46]. Daruwalla A, Zhang J, Lee HJ, Khadka N, Farquhar ER, Shi W, von Lintig J, and Kiser PD (2020) Structural basis for carotenoid cleavage by an archaeal carotenoid dioxygenase, Proc Natl Acad Sci U S A 117, 19914–19925. [PubMed: 32747548]

[47]. Nagao A, Maoka T, Ono H, Kotake-Nara E, Kobayashi M, and Tomita M (2015) A 3-hydroxy beta-end group in xanthophylls is preferentially oxidized to a 3-oxo epsilon-end group in mammals, J Lipid Res 56, 449–462. [PubMed: 25502844]

[48]. Hessel S, Eichinger A, Isken A, Amengual J, Hunzelmann S, Hoeller U, Elste V, Hunziker W, Goralczyk R, Oberhauser V, von Lintig J, and Wyss A (2007) CMO1 deficiency abolishes vitamin A production from beta-carotene and alters lipid metabolism in mice, J Biol Chem 282, 33553–33561. [PubMed: 17855355]

[49]. Widjaja-Adhi MA, Lobo GP, Golczak M, and Von Lintig J (2015) A genetic dissection of intestinal fat-soluble vitamin and carotenoid absorption, Human molecular genetics 24, 3206–3219. [PubMed: 25701869]

[50]. Waterhouse A, Bertoni M, Bienert S, Studer G, Tauriello G, Gumienny R, Heer FT, de Beer TAP, Rempfer C, Bordoli L, Lepore R, and Schwede T (2018) SWISS-MODEL: homology modelling of protein structures and complexes, Nucleic Acids Res 46, W296–W303. [PubMed: 29788355]

[51]. Emsley P, and Cowtan K (2004) Coot: model-building tools for molecular graphics, Acta Crystallogr D Biol Crystallogr 60, 2126–2132. [PubMed: 15572765]

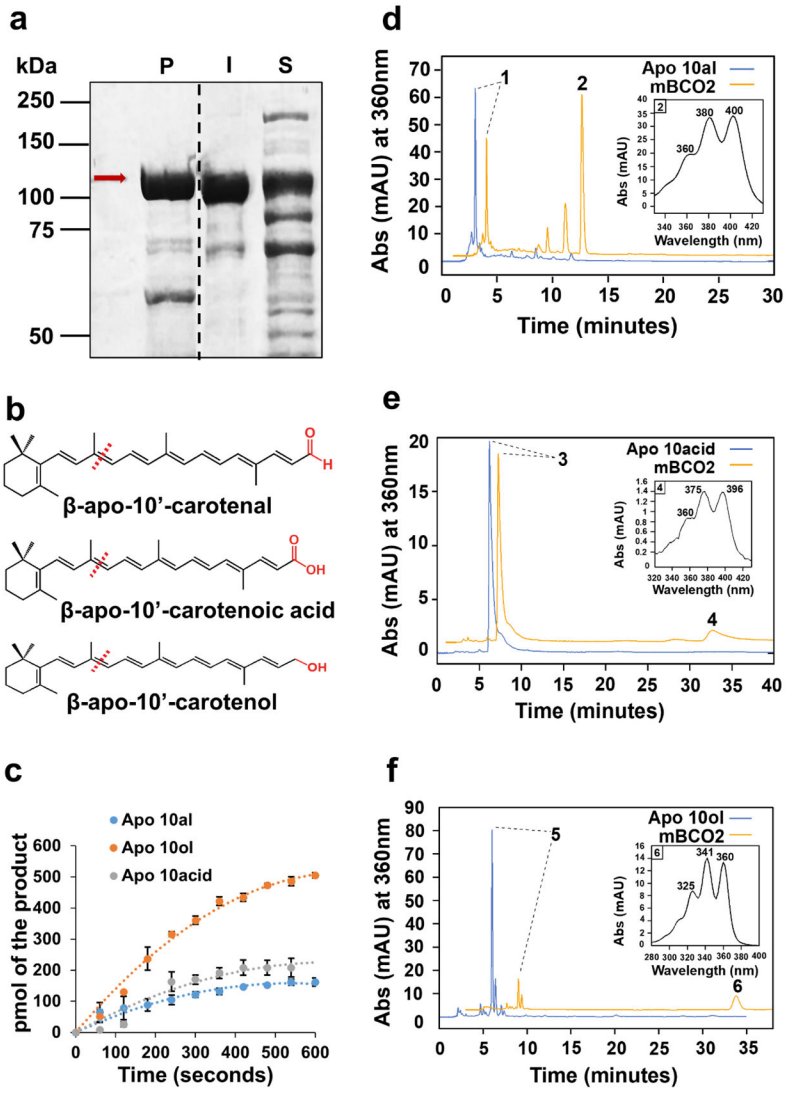

Figure 1.

mBCO2 converts β-apocarotenoid substrates with different polar end groups. a) SDS-PAGE of MBP-mBCO2 protein (mBCO2) purification, P indicates protein fractions eluted from the column, I indicates insoluble protein in cell pellet, and S indicates soluble protein in crude extract. Red arrow points to mBCO2 fusion protein. b) Structures of β-apocarotenoids. Functional groups (carboxylic acid, aldehyde, and alcohol) are highlighted in red. c) Enzyme kinetics of mBCO2 (50 μg) with different substrates. The initial velocity was 77.3 pmol x min^{-1} for β-apo-10'-carotenol, 39.6 pmol x min^{-1} for β-apo-10'-carotenoic acid, and 21.1 pmol x min^{-1} for β-apo-10' carotenal. The experiment was repeated three time and the values are displayed as mean +/− standard deviation. d,e,f) HPLC traces at 360 nm of lipid extracts of enzyme assays with (orange trace) and without (blue trace) mBCO2. The insets show the UV visible spectrum of the respective products. In d) peak 1 is β-apo-10'-carotenal, peak 2 is 10',10-apocarotene-dialdehyde, in e) peak 3 is β-apo-10'-carotenoic acid, peak 4 is 10-oxo-10,10'-diapocaroten-10'-oic acid, in f) peak 5 is β-apo-10'-carotenol, and peak 6 is 10-Oxo-10,10'-diapocaroten-10'-ol.

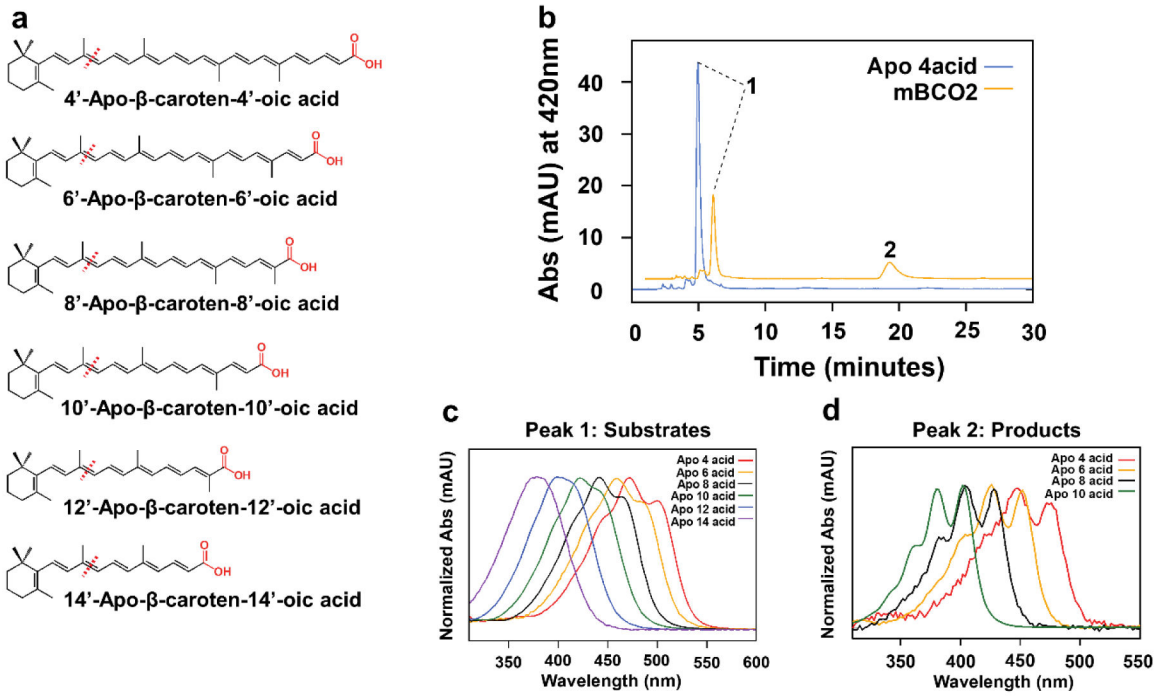

Figure 2.

mBCO2 converts β-apo-carotenoic acids with various chain length. a) Chemical structures of the β-apo-carotenoic acid substrates with different chain length. Expected cleavage sites are indicated with red dashed lines. The carboxylic end groups are highlighted in red. b) Representative HPLC of lipid extracts of reactions with β-apo-4'-carotenoic acid incubated in the presence (orange trace) and absence (blue trace) of mBCO2. Peak 1 is β-apo-4'-carotenoic acid and peak 2 is 10-Oxo-10,4'-diapocarotene-4'-oic acid. c) Representative UV-visible absorption spectra of β-apo-carotenoic acid substrates. d) Representative UV-visible absorption spectra of diapocarotenoid products from enzyme assays with mBCO2.

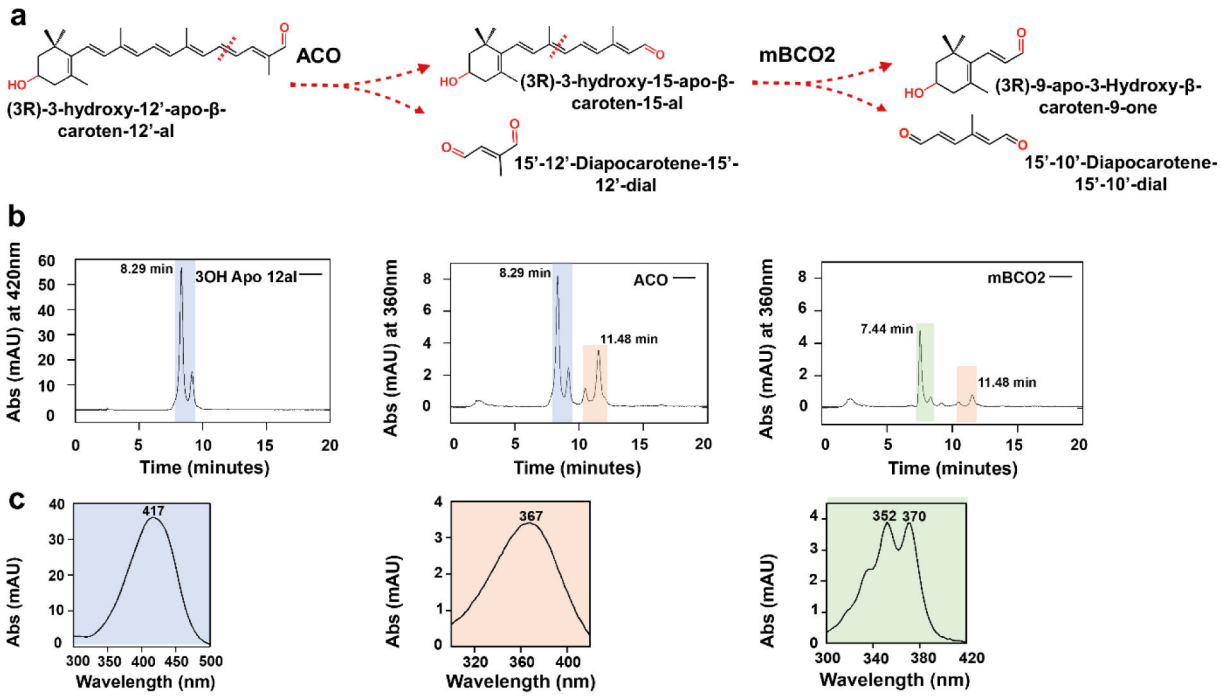

Figure 3.

mBCO2 converts 3-hydroxy-retinal after being generated by ACO. a) Reaction scheme for the successive conversion of 3-hydroxy-β-apo-12'-carotenal by ACO to 3-hydroxy-retinal, followed by the conversion of 3-hydroxy-retinal to 3-hydroxy-β-ionone. b) HPLC traces of enzyme assays with ACO and mBCO2. Left panel displays the HPLC trace at 420 nm of the 3-hydroxy-β-apo-12'-carotenal substrate (retention time, 8.29 min); middle panel displays HPLC trace at 360 nm of an enzyme assay with 3-hydroxy-β-apo-12'-carotenal and ACO which results in 3-hydroxy-retinal (retention time, 11.48 min) formation; right panel displays HPLC trace at 360 nm of an enzyme assays in which the 3-hydroxy-retinal produced by ACO was incubated in the presence of mBCO2. Note that this incubation results in the disappearance of the 3-hydroxy-retinal peak. Additionally, 10',10-apocarotene-dialdehyde (retention time, 7,44 min) is produced by the conversion of the remaining 3-hydroxy β apo-12'-carotenal substrate. c) UV-Visible spectra of peak 1, 3-hydroxy-β-apo-12'-carotenal, peak 2, 3-hydroxy-retinal and peak 3, 12',10-apocarotene-dialdehyde. The *cis* isomer of 3-hydroxy-β-apo-12'-carotenal substrate elutes next to the major substrate peak.

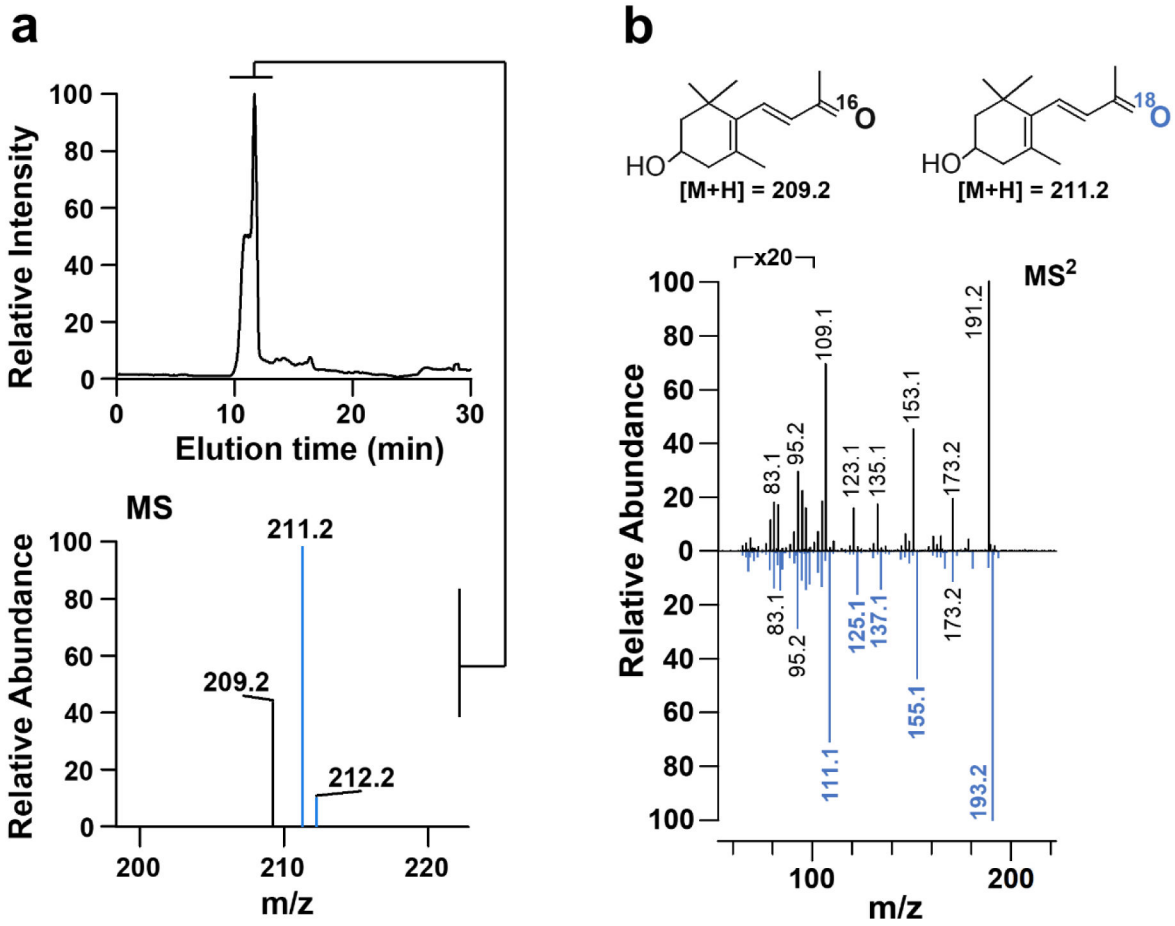

Figure 4.

Murine BCO2 is a dioxygenase. a) LC-MS analysis of $^{18}O_2$ incorporation into the 3-hydroxy-ionone product of 3-hydroxy- β –apo-12'-carotenal cleavage by mBCO2. b) MS/MS spectra of the two 3-hydroxy-β-ionone isotopologues.

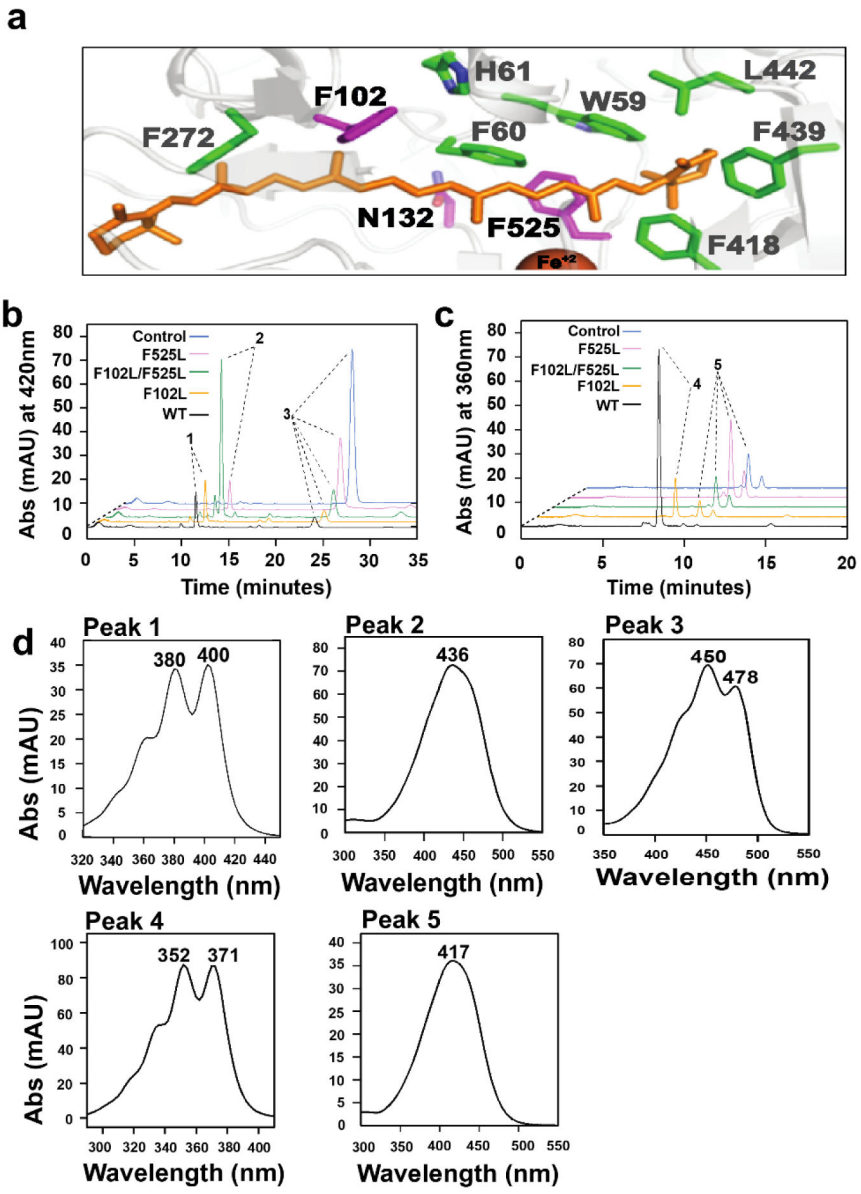

Figure 5.

BCO2 possesses a bipartite substrate binding cavity which discriminates between carotenoids and apocarotenoids. a) Close up view of the modeled substrate binding cavity of BCO2 with bound β-carotene (orange). The cavity is lined with aromatic amino acid side residues (green) which are conserved between BCO1 and BCO2. Mutated amino acid residue F102, N132 and F525 are highlighted in magenta. b) HPLC traces at 420 nm of enzyme assays of wild type and mutant mBCO2 variants incubated with meso-zeaxanthin. In control experiments, the substrate was incubated with maltose binding protein c) HPLC traces at 360 nm of enzyme assays of wild type and mutant BCO2 variants incubated with 3-hydroxy-β-apo-12'-carotenal. In control experiments, the substrate was incubated with maltose binding protein. d) UV-visible spectra of major products' peaks in B and C. Peak 1is

10’,10-apocarotene-dialdehyde; peak 2 is 3-β-apo-10’ carotenal, peak 3 is meso-zeaxanthin; peak 4 is 12’,10-apocarotene-dialdehyde; peak 5 is 3-hydroxy-β-apo-12’-carotenal.

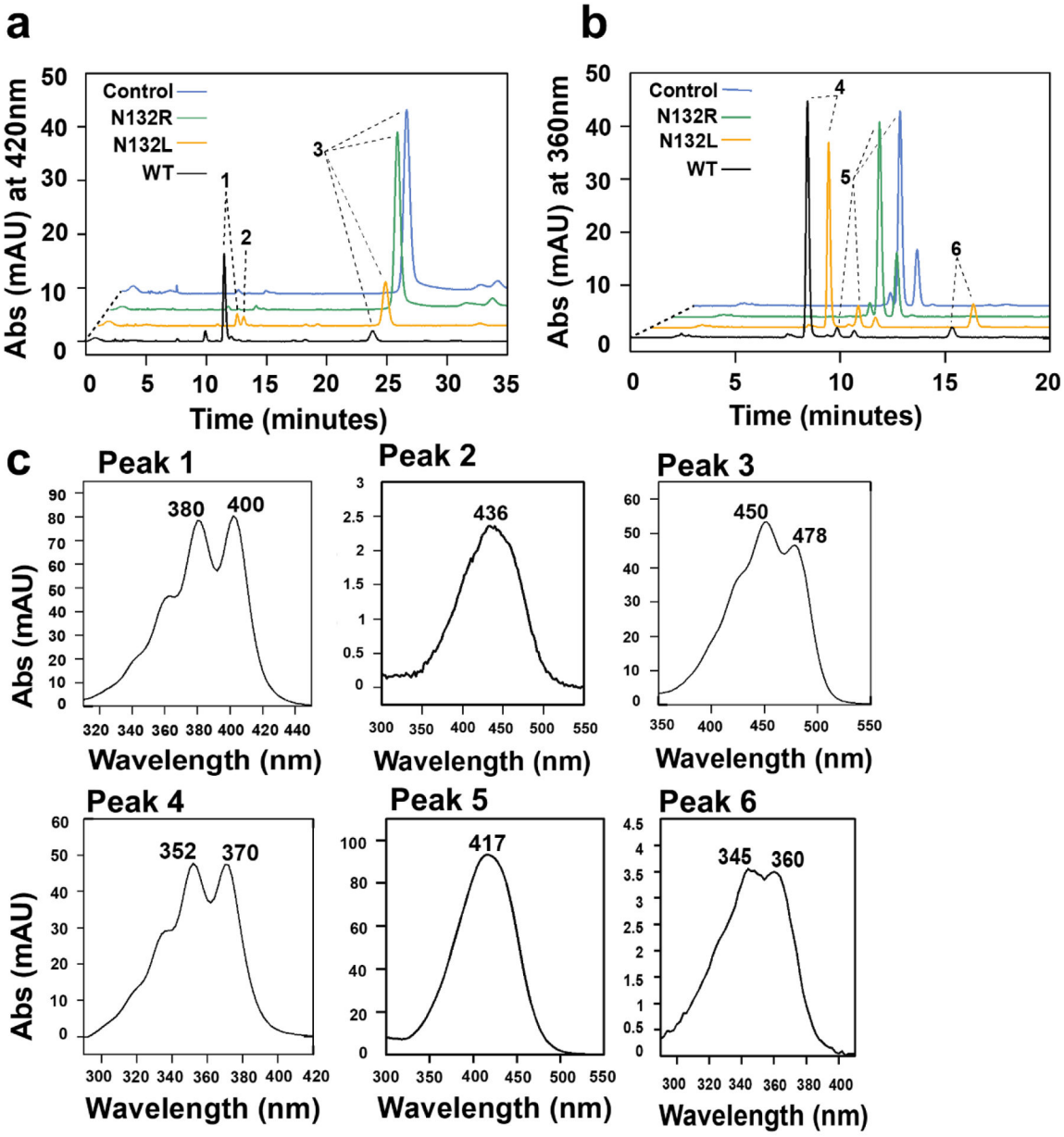

Figure 6.

Asn132 stabilizes π electron bonding in the active center of BCO2. a) HPLC traces at 420 nm of enzyme assays of wild type and mutant mBCO2 variants incubated with meso-zeaxanthin. In control experiments, the substrate was incubated with maltose binding protein b) HPLC traces at 360 nm of enzyme assays of wild type and mutant mBCO2 variants incubated with 3-hydroxy-β-apo-12'-carotenal. In control experiments, the substrate was incubated with maltose binding protein. c) UV-visible spectra of products and substrates. peak 1, 10',10-apocarotene-dialdehyde; peak 2, beta-apo-10'-carotenal; peak 3, meso-zeaxanthin; peak 4, 12',10-apocarotene-dialdehyde; peak 5, 3 hydroxy-β-apo-12'-carotenal; peak 6, 10',10-apocarotene-diol.

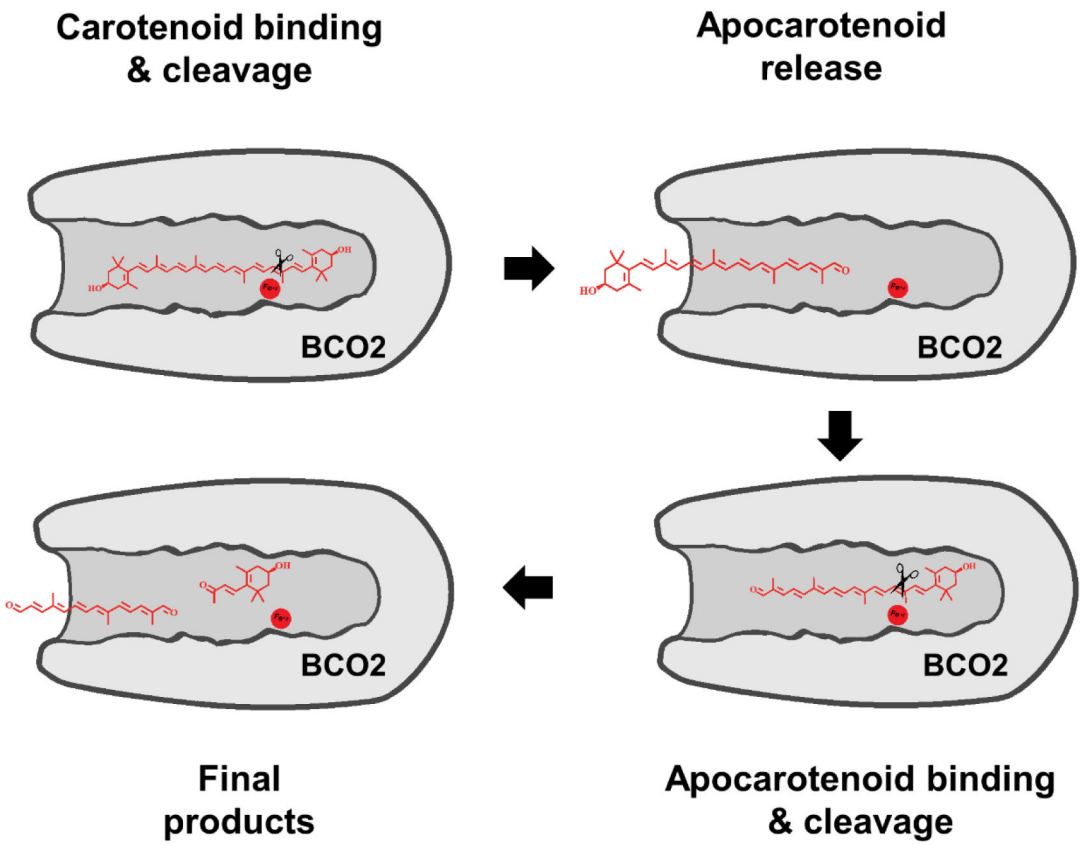

Figure 7.

Cartoon of the different steps of carotenoid cleavage by BCO2. The carotenoid molecule enters the substrate-binding tunnel. Cleaves at the 9,10 double bond results in the removal of one ionone ring site and the formation of an apocarotenoid. The apocarotenoid product leaves the substrate-binding cavity. The apocarotenoid then reenters the substrate-binding cavity in reverse direction followed by cleavage at the 9',10' double bond position. The results in the removal of the second ionone ring site and the formation of a diapocarotenoid product.

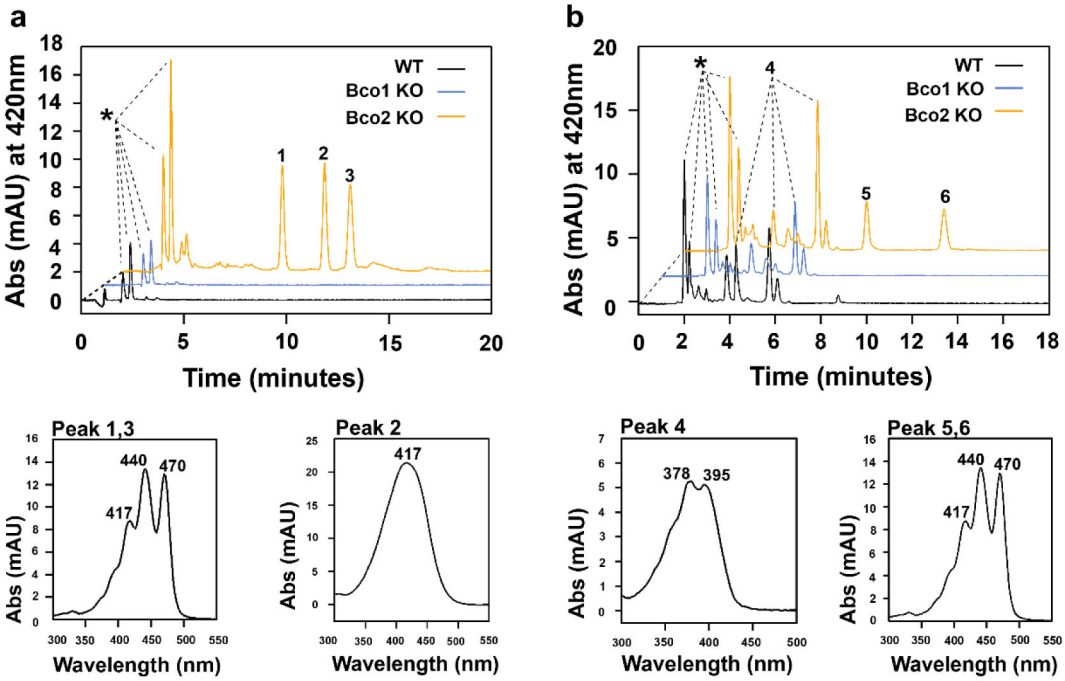

Figure 8.

Apocarotenoids accumulate in BCO2-deficient mouse liver. a) HPLC traces at 420 nm of lipid extracts of mice gavaged with 3-hydroxy-β-apo-12'-carotenal. The peaks indicated by asterisks are retinoid peaks (retinyl esters and all-*trans*-retinol). Lower left panel is UV-visible absorption spectra of unknown dietary compounds (peak 1 and 3) and lower right panel is 3-hydroxy-β-apo-12'-carotenal (peak 2). b) HPLC traces of lipid extracts of mice gavaged with β-apo-10'-carotenal. The peaks indicated by asterisks are retinoid peaks (retinyl esters and all-*trans*-retinol). Lower left panel is UV-visible absorption spectra of β-apo-10'-carotenol (peak 4) and lower right panel is the two unknown dietary compounds (peaks 5 and 6).